Investigation and modelling of rubber stationary friction on rough surfaces

2008 J. Phys.: Condens. Matter 20 015007

(http://iopscience.iop.org/0953-8984/20/1/015007)

IOP PUBLISHING JOURNAL OF PHYSICS: CONDENSED MATTER

J. Phys.: Condens. Matter **20** (2008) 015007 (13pp) doi:10.1088/0953-8984/20/01/015007

Investigation and modelling of rubber stationary friction on rough surfaces

A Le Gal and M Klüppel[1]

Deutsches Institut für Kautschuktechnologie, Eupener Straße 33, D-30519 Hannover, Germany

E-mail: manfred.klueppel@dikautschuk.de

Received 5 July 2007, in final form 14 September 2007
Published 12 December 2007
Online at stacks.iop.org/JPhysCM/20/015007

Abstract

This paper presents novel aspects regarding the physically motivated modelling of rubber stationary sliding friction on rough surfaces. The description of dynamic contact is treated within the framework of a generalized Greenwood–Williamson theory for rigid/soft frictional pairings. Due to the self-affinity of rough surfaces, both hysteresis and adhesion friction components arise from a multi-scale excitation of surface roughness. Beside a complete analytical formulation of contact parameters, the morphology of macrotexture is considered via the introduction of a second scaling range at large length scales which mostly contribute to hysteresis friction. Moreover, adhesion friction is related to the real area of contact combined with the kinetics of interfacial peeling effects. Friction experiments carried out with different rubbers on rough granite and asphalt point out the relevance of hysteresis and adhesion friction concepts on rough surfaces. The two scaling ranges approach significantly improves the description of wet and dry friction behaviour within the range of low sliding velocity. In addition, material and surface effects are predicted and understood on a physical basis. The applicability of such modelling is of high interest for materials developers and road constructors regarding the prediction of wet grip performance of tyres on road tracks.

(Some figures in this article are in colour only in the electronic version)

1. Introduction and motivation

Friction is a fundamental physical phenomenon of high technological importance for a wide range of applications. Since friction arises from the relative motion of two bodies put in contact with one another, the effect is inherent to all mechanical systems involved in the transmission of forces or torques. Consequently, friction takes place in almost all components of power machines subjected to dynamic stresses, be it engine gears or during the contact wheel/rail or tyre/road. Thereby, the nature of frictional pairings is crucial for the description of dynamic contact problems.

The particular case of rubber friction on rough surfaces displays a complex physical process and challenging situation from the modelling point of view. This is due to the versatile thermomechanical behaviour of elastomers combined with the random nature of surface roughness. As a result, the prediction of traction properties of tyres under wet conditions based on laboratory data stills remains an extremely difficult task. One reason is the insufficient analytical description of dynamic contact problems and the resulting friction phenomenon between elastomers and rough, rigid substrates.

Elastomers belong to the family of polymer materials, e.g. their microstructure basically relies on the entanglements of long macromolecular chains. They mainly differ from their glass transition temperature which is located below room temperature, indicating that elastomers exhibit a soft state at moderate temperatures under static conditions. One of the main advantages of rubber is that a wide range of target physical properties can be tailored by the addition of chemical components: a small amount of sulfur combined with high temperatures leads to the formation of a three-dimensional network with chemical bonds between polymer chains, e.g. significantly improves the elasticity. If fillers (carbon black, silica) are incorporated into the polymer matrix, dynamic mechanical and thermal properties are dramatically modified due to the occurrence of physical interactions associated with the filler network [1].

[1] Author to whom any correspondence should be addressed.

When a rubber block slides on a rough substrate, the indentation process originating from surface asperities causes a periodical deformation of the elastomer related to internal losses. This energy dissipation mechanism induced during dynamic contact is denoted as hysteresis friction in the literature and found to be meaningful with increasing roughness amplitude. At the same time, the intimate contact down to small length scales suggests the occurrence of adhesive bonds. Thus, sliding friction can be seen as the successive formation and breakage of contact patches distributed over the nominal contact area which gives an additional contribution on the friction coefficient, namely adhesion friction. Since both components are associated with dynamic mechanical properties of elastomers, rubber friction on rough surfaces was found to exhibit typical viscoelastic features [2]. Accordingly, the position of the friction maximum was found to be intimately correlated with the frequency dependent dynamic modulus. Furthermore, the existence of hysteresis and adhesion friction on rough surfaces could be demonstrated, whereby the level of adhesion is strongly influenced by the nature of contact conditions [2]. Consequently, rubber friction is expected to vary with sliding velocity, load, temperature, surface morphology and elastomer formulation.

Novel modelling of hysteresis and adhesion friction consider self-affine properties of surfaces, e.g. morphological invariance under anisotropic dilations, which means that surface roughness is considered over many length scales. The applicability of fractal concepts has been demonstrated for road surfaces leading to the establishment of empirical correlations between surface descriptors and traction properties of tyres during ABS-braking phases [6]. The consideration of self-affinity led to the recent development of hysteresis friction models in which energy losses generated by the roughness spectrum during dynamic contact are expressed as a friction integral over a range of excitation frequencies [3–8].

This paper presents further extensions regarding the modelling of rubber stationary sliding friction properties on rough self-affine surfaces already presented in the literature [6, 16]. In particular, the applicability of multi-scaling concepts for the description of friction values under wet and dry conditions is addressed for filled and unfilled elastomers. Based on the Greenwood–Williamson contact theory, a semi-analytical procedure is presented for the description of the upper part of rough profile where contact actually occurs. This is of considerable importance for the calculation of contact parameters governed by the largest length scales of profile. Furthermore, the decomposition of roughness into two texture regimes leads to an extended analytical formulation of the hysteresis friction coefficient whereby the contribution of both microtexture and macrotexture are quantitatively evaluated. In addition, adhesion friction is expressed as the computed real area of contact combined with a velocity dependent interfacial shear strength arising from the kinetics of peeling effects on small length scales. Stationary friction tests carried out at moderate load within the range of low sliding velocity highlight the relevance of hysteresis and adhesion friction concepts on rough surfaces for filled and unfilled S-SBR grades. Finally, numerical parameters and results of unfilled composites are exhaustively discussed.

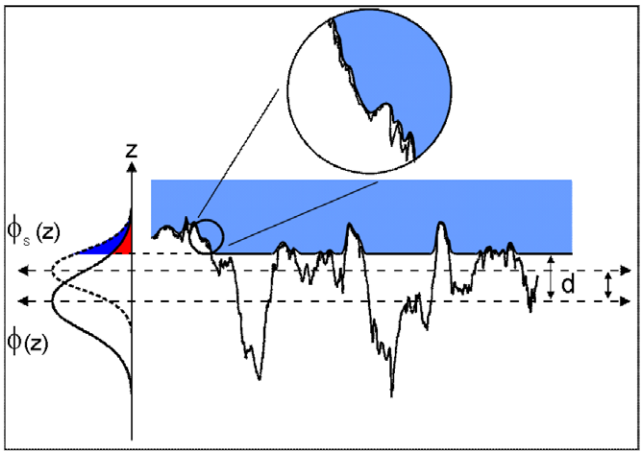

Figure 1. Rough profile with associated height distribution $\phi(z)$ and summit distribution $\phi_s(z)$. Reproduced with permission from [20].

2. Contact mechanics and rubber friction on rough surfaces

2.1. Contact mechanics on rough surfaces

The dynamic contact between elastomers and rough rigid surfaces is analytically treated on the basis of the Greenwood–Williamson theory [11]. Thereby, the surface is approximated by spheres with a single radius R and vertically distributed according to a height distribution $\phi(z)$. As a result, the load F_N is expressed as the sum of N distinct contact forces $F_{n,i}$ of Hertzian type in dependence of the distance d between the rubber surface and the mean height $\langle z \rangle$ of the surface formed by the spherical summits of radius R. Since the contact only involves the upper fraction of the rough surface, the fraction of the profile contributing to the normal force is characterized by a second height distribution denoted by $\phi_s(z)$ as illustrated in figure 1. A simple extension of the elastic contact derived by Greenwood and Williamson to rubber friction problems can be achieved by introducing the dynamic complex modulus $E^*(\omega)$ describing the frequency dependent behaviour of viscoelastic materials. In a first approximation, rubber can be assumed to be incompressible ($\nu = 0.5$) and the normal force F_N is given by [11]:

$$F_N = \sum_{i=1}^{N} F_{n,i} = \tfrac{16}{9} N |E^*(\omega)| R^{1/2} \int_d^\infty (z-d)^{3/2} \phi_s(z)\, dz. \quad (1)$$

The decomposition of normal force has to be carefully treated for multiple-scale contact problems. Indeed, the theory of Greenwood and Williamson is based on the assumption that two neighbouring asperities act independently on the counter solid. For rough surfaces, this condition is clearly not satisfied at a certain length scale below which local deformation fields tend to overlap. Thus, statistically averaged and length scale dependent quantities like the mean asperity

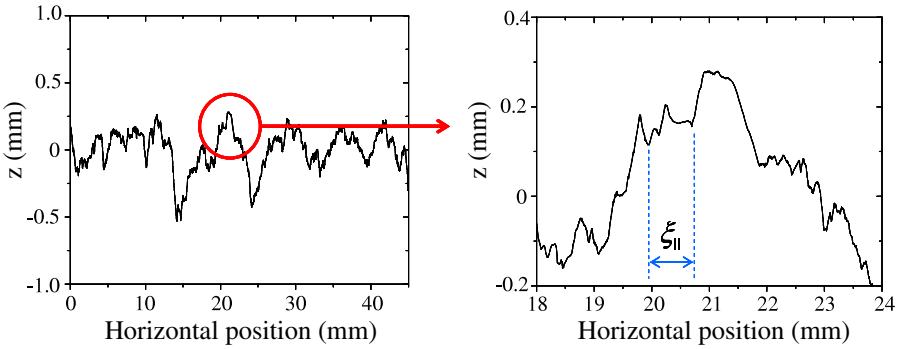

Figure 2. Original rough profile (left) and magnified region (right).

curvature or the real area of contact can not be evaluated within the frame of the Greenwood–Williamson theory in its basic form and the applicability of the Greenwood–Williamson approximation yields only for contact parameters governed by the largest roughness scales of the profile, for example the mean penetration depth $\langle z_p \rangle$ and the corresponding normal stress σ_0.

The evaluation of contact forces requires the determination of the summit height distribution $\phi_s(z)$ characterizing the fraction of profile contacting with the rubber. Based on an analytical formulation combined with a numerical procedure, a method has been proposed for the estimation of the summit height distribution $\phi_s(z)$. An affine transformation associated with an affine parameter s is introduced to describe the shift of the original height distribution $\phi(z)$ towards higher region of the profile. Be the upper boundary z_{max} fixed, each point of the profile with a height z will be transformed according to the following relationship:

$$z_s = \frac{(z - z_{max})}{s} + z_{max} \tag{2}$$

where z_s is the transformed height. The new standard deviation of $\phi_s(z)$ is given by:

$$\tilde{\sigma}_s = \frac{\tilde{\sigma}}{s} \tag{3}$$

with $\tilde{\sigma}$ being the standard deviation of $\phi(z)$. The mean value $\langle z_s \rangle$ of $\phi_s(z)$ follows as:

$$\langle z_s \rangle = z_{max}\left(1 - \frac{1}{s}\right). \tag{4}$$

On the other side, a numerical procedure calculates the local maxima distribution of a profile with various interval lengths. The principle is depicted in figure 2. For small length intervals in the range of the measurement resolution, the maxima distribution tends to the original height distribution $\phi(z)$. By increasing the interval length, the procedure eliminates the valleys where no contact occurs and only retains the highest region of profile. In particular, the maxima distribution associated with an interval length $\xi_\parallel$ corresponds to the approximation of Greenwood–Williamson where macroasperities are replaced by spheres. For these quantities, the surface can reasonably be approximated by spheres corresponding to the largest asperity, e.g. with a diameter $\xi_\perp$ and separated by a distance $\xi_\parallel$.

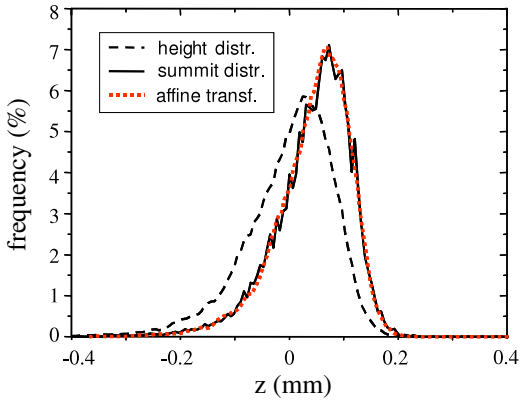

Figure 3. Comparison between the original distribution, the numerical maxima distribution and the analytical affine distribution for a corundum surface. The best fit is obtained for the parameter $s = 1.20$.

An example of the maxima distribution is shown in figure 3 for a corundum surface with an interval length corresponding to the horizontal cut-off length $\xi_\parallel$ of the surface. As expected, a shift of the mean value is observed which indicates that only the upper part of the profile is taken into account. Accordingly, the shape of the distribution is narrower compared to the original distribution. As a comparison, the analytical affine transformed distribution is shown with an affine parameter found to be $s = 1.20$. A fairly good agreement can be seen between both methods which allows an analytical formulation of the summit height distribution $\phi_s(z) = f(\phi(z))$, with the affine parameter as a characteristic of each surface.

2.2. *Self-affinity of rough surfaces*

The fractal nature of many surfaces has been studied within the last twenty years [13–15]. It appears that most of engineered surfaces of practical importance exhibit a self-affine behaviour. The term self-affinity yields for objects which show an invariance of the morphology and statistical properties under anisotropic dilations [12]. For such surfaces,

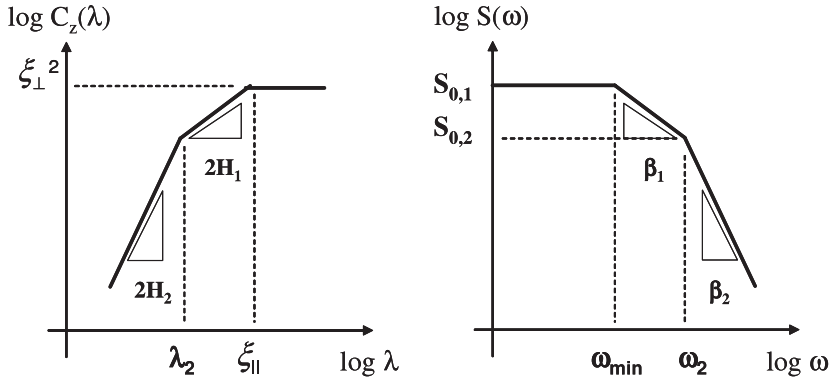

Figure 4. Schematic representation of the height difference correlation function $C_z(\lambda)$ and power spectrum density $S(\omega)$ with a two scaling ranges approach.

a vertical cross-section magnified by a scaling factor α in the xy plane and by a factor α^H (where $0 < H < 1$) in the perpendicular direction remains statistically invariant. H is denoted as the Hurst exponent and describes the degree of the surface irregularity. It is related to the local fractal dimension D by the equation $D = 3 - H$.

Many engineered surfaces show a self-affine behaviour within a defined wave length interval. The upper cut-off length is identified with the largest surface corrugations: for road surfaces, this corresponds to the limit of macrotexture, e.g. the aggregate size. On the other side, the lower cut-off length is fundamentally limited by the spatial resolution of the measuring equipment. The main experimental difficulty arises from the necessity to achieve a proper characterization of the microtexture (micrometre range) while encompassing the largest asperities of the profile in the height up to a few millimetres. Consequently, the characterization of self-affine properties is fundamentally limited by both the investigated surface and the measuring equipment. Macroscopically rough surfaces like roads exhibit fractal dimensions comprised between $D = 2$ and 2.5, whereby the D-value was found to strongly vary with the type of roughness analysis [20].

The self-affine character of a surface is mathematically treated by correlation functions, for instance the height difference correlation function $C_z(\lambda)$. It calculates the mean square height fluctuations of the surface with respect to the horizontal length scale λ and is given by:

$$C_z(\lambda) = \langle (z(x+\lambda) - z(x))^2 \rangle \tag{5}$$

where $z(x)$ accounts for the profile height at a horizontal position x and $\langle \cdots \rangle$ is the average over the set of observation.

Recent investigations of road surfaces showed a clear deviation between a single scaling behaviour of roughness properties and the statistical height difference correlation function at sufficiently high λ-values [6, 20, 21]. This suggests that large length scales exhibit different morphological properties than the one characterizing the range of microtexture. This remark has practical implications on the modelling of roughness: indeed, road surfaces are known to be dominated by two main scaling regimes interpreted in terms of texture. The macrotexture is related to the morphology of largest asperities—depending on granulate or aggregate size—while the microtexture rather describes their surface state, namely grain process, polishing, or abrasion. Moreover, microtexture and macrotexture are both associated with determining—but distinct—physical mechanisms regarding the dynamic contact tyre/road during friction processes under dry and wet conditions. The level of macrotexture—from fine to coarse—controls the rate at which friction decreases at high sliding velocities under wet conditions by promoting the drainage ability of the surface and therefore reducing the risk of aquaplaning. On the other side, the type of microtexture—polished, rough—appears to control the level of friction, e.g. asperities at small length scales offer additional contact possibilities during dynamic contact. Physically, local high pressures due to microroughness are likely to cause the breakage of the interfacial water film and the formation of dry contact islands which finally increases the level of friction. Hence, while the influence of microasperities is marginal under dry conditions, it considerably improves the skid resistance under wet conditions.

Since large length scales mostly contribute to hysteresis friction, a fine characterization of macrotexture is required in order to obtain relevant simulations of the friction behaviour. Consequently, the height difference correlation function is decomposed into two distinct scaling regimes as shown in figure 4. It yields:

$$C_Z(\lambda) = \xi_\perp^2 \left(\frac{\lambda}{\xi_\parallel}\right)^{2H_1} \qquad \text{for } \lambda_2 < \lambda < \xi_\parallel, \tag{6}$$

where λ_2 is the boundary length corresponding to the crossover of both scaling ranges. For the second scaling range, the height difference correlation function $C_z(\lambda)$ is given by:

$$C_Z(\lambda) = \xi_\perp^2 \left(\frac{\lambda}{\lambda_2}\right)^{2H_2} \left(\frac{\lambda_2}{\xi_\parallel}\right)^{2H_1} \qquad \text{for } \lambda < \lambda_2 \tag{7}$$

with $\xi_\perp$ and $\xi_\parallel$ being the vertical and horizontal cut-off length of the surface roughness, respectively.

A similar approach can be applied to the power spectrum density $S(\omega)$ in the frequency space (see figure 4). For the

largest length scales, one obtains:

$$S_1(\omega) = S_{0,1}\left(\frac{\omega}{\omega_{\min}}\right)^{-(7-2D_1)} \quad \text{for } \omega_{\min} < \omega < \omega_2,$$
$$S_{0,1} = \frac{(3-D_1)\xi_\perp^2}{2\pi\upsilon\xi_\parallel} \tag{8}$$

where $\omega_{\min} = 2\pi\upsilon/\xi_\parallel$, $\omega_2 = 2\pi\upsilon/\lambda_2$, with υ denoting the sliding velocity.

For the second scaling range, it yields:

$$S_2(\omega) = S_{0,2}\left(\frac{\omega}{\omega_c}\right)^{-(7-2D_2)} \quad \text{for } \omega_2 < \omega,$$
$$S_{0,2} = \frac{(3-D_1)\xi_\perp^2}{2\pi\upsilon\xi_\parallel}\left(\frac{\omega_{\min}}{\omega_c}\right)^{(7-2D_1)} \tag{9}$$

where $S_{0,2}$ is found to be directly related to the plateau value $S_{0,1}$. A general formulation of the height difference correlation function and power spectrum density for n-scaling ranges is developed in [18].

2.3. Modelling of hysteresis friction—two scaling regimes

Hysteresis friction arises from the energy dissipation caused by the local deformation of rubber by surface asperities during sliding process. Due to the self-affine nature of rough surfaces, the hysteresis friction coefficient is integrated over a range of excitation frequency corresponding to multi-scale indentation mechanisms during the sliding process. It has been seen that the introduction of multi-fractality concepts implies a generalized formulation for both the height difference correlation function $C_z(\lambda)$ and the power spectrum density $S(\omega)$. Consequently, the hysteresis friction integral initially presented in [6] is decomposed into two terms associated with each scaling regime. The contact parameters that were calculated in the frame of the extended Greenwood–Williamson theory are not affected by the number of scaling regimes—for instance the mean penetration depth $\langle z_p\rangle$. Consequently, for a two scaling ranges approach, the hysteresis friction coefficient μ_H is given by:

$$\mu_H \equiv \frac{F_H}{F_N} = \frac{1}{2}\frac{\langle\delta\rangle}{\sigma_0\upsilon}\left\{\int_{\omega_{\min}}^{\omega_2} \mathrm{d}\omega\,\omega E''(\omega)S_1(\omega) + \int_{\omega_2}^{\omega_{\max}} \mathrm{d}\omega\,\omega E''(\omega)S_2(\omega)\right\}. \tag{10}$$

Here $\langle\dot{\delta}\rangle$ is the excited layer thickness ($\langle\dot{\delta}\rangle \sim \langle\dot{z}_p\rangle \sim F_1(t)$) and σ_0 is the load ($\sigma_0 \sim F_{3/2}(t_s)$).

$S_1(\omega)$ and $S_2(\omega)$ are the power spectrum density of macrotexture and microtexture, respectively, as previously determined in equations (8) and (9). $\omega_2 = 2\pi\upsilon/\lambda_2$ is determined via the crossover of the two scaling regimes. A generalized formulation of the hysteresis friction coefficient and corresponding contact parameters for n-scaling ranges is presented in [18].

The modelling of roughness with two scaling ranges has strong implications on the formulation of length scale dependent contact parameters, e.g. the real area of contact and the contact interval. A detailed presentation of calculation steps is shown in [18]. As a result, the smallest length scale $\lambda_{\min}$ contributing to hysteresis friction with a two scaling ranges approach is given by:

$$\frac{\lambda_{\min}}{\xi_\parallel} \cong \left(\left(\frac{\lambda_2}{\xi_\parallel}\right)^{3(D_2-D_1)} \frac{0.09\pi s^{3/2}\xi_\perp |E(\lambda_{\min})| F_0(t)\tilde{n}_s}{\xi_\parallel |E(\xi_\parallel)| F_{3/2}(t_s)}\right)^{\frac{1}{3D_2-6}} \tag{11}$$

with the abbreviations $\tilde{n}_s = 6\pi\sqrt{3}\lambda_c^2 n_s$ and $F_n = \int_t^\infty (x-t)^n \phi(x)\,\mathrm{d}x$ for $n = 0, 1, 3/2$.

Here $\xi_\parallel$ accounts for the horizontal cut-off length, λ_2 is the crossover length scale between macrotexture and microtexture, D_1 and D_2 correspond to the fractal dimension of macrotexture and microtexture, respectively. $F_0(t)$ and $F_{3/2}(t_s)$ are the Greenwood–Williamson (GW) functions with $t \equiv d/\tilde{\sigma}$ and $t_s \equiv d/\tilde{\sigma}_s$, respectively. n_s denotes the summit density and λ_c accounts for the lowest cut-off length of surfaces, typically $\lambda_c \sim 10^{-10}$ m, where a crossover from the fractal disorder to the atomic ordered structure appears. $E(\lambda_{\min})$ and $E(\xi_\parallel)$ are the dynamic moduli at respective frequency $\omega = 2\pi\upsilon/\lambda_{\min}$ and $\omega = 2\pi\upsilon/\xi_\parallel$, υ being the sliding velocity.

Consequently, the corresponding real area of contact $A_c(\lambda_{\min})$ at a length scale $\lambda_{\min}$ is given by [18]:

$$A_c(\lambda_{\min}) \approx A_0\left(\frac{\xi_\parallel F_0^2(t) F_{3/2}(t_s)|E(\xi_\parallel)|\tilde{n}_s^2}{808\pi s^{3/2}\xi_\perp |E(\lambda_{\min})|}\right)^{\frac{1}{3}} \tag{12}$$

where a short analysis shows that $\tilde{n}_s \sim (3-\beta_2)/(5-\beta_2)$, e.g. the correction term compared to a one scaling range approach is solely influenced by the fractal dimension of microtexture.

We point out that the contact theory described by equations (11) and (12) takes into account the real height distribution via the GW functions $F_0(t)$ and $F_{3/2}(t_s)$. This is important for practical applications, since the GW functions may differ significantly for various surfaces leading e.g. to a different load dependence of the hysteresis friction coefficient $\mu_H \sim F_1(t)/F_{3/2}(t_s)$ [18, 22]. In particular, the impact of the real height distribution on the dynamic contact becomes significant in the every day situation of worn (more or less abraded) road tracks, which often exhibit a strongly asymmetric height distribution [22]. In this case the assumption of statistically rough surfaces with a symmetric (Gaussian) height distribution (compare e.g. [8]) is not appropriate for describing the surface roughness since the alterations of the contact mechanics and the friction characteristics due to the asymmetric height distribution cannot be neglected [22].

2.4. Modelling of adhesion friction

Beside the hysteresis component, adhesion is the most significant contribution to rubber friction on rough surfaces as long as wear and hydrodynamic effects are negligible during sliding process. Basically, adhesion can even take place during rubber sliding friction on wet rough surfaces. The presence of lubricant is a *necessary* but not *sufficient* condition for the suppression of adhesion [10]. The breakage

of lubricant film during the sliding process is activated by the surface microtexture and might lead to the formation of statistically distributed islands of dry contact under wet conditions. This mechanism appears to be strongly dependent on the nature of the lubricant, morphology of the roughness and can be hindered by detergents which are known to prevent intimate contact between rubber and rough substrate. Under dry conditions, both hysteresis and adhesion components contribute to the frictional process.

By following the widely accepted decomposition of the friction coefficient μ into hysteresis and adhesion components, the adhesion friction coefficient μ_{Adh} is given by [2, 10, 16]:

$$\mu = \mu_{\mathrm{H}} + \mu_{\mathrm{Adh}}, \qquad \text{with } \mu_{\mathrm{Adh}} = \frac{F_{\mathrm{Adh}}}{F_{\mathrm{N}}} = \frac{\tau_{\mathrm{s}}}{\sigma_0} \cdot \frac{A_{\mathrm{c}}}{A_0} \quad (13)$$

where F_{Adh} is the contribution on friction force arising from interfacial processes, σ_0 accounts for the load, A_{c}/A_0 denotes the fractional area which can be predicted according to equation (12). Through this convenient formulation, the level of adhesion friction is determined by a single free parameter, namely the true interfacial shear strength τ_{s} describing the local force required to break contact junctions.

Following previous investigations carried out on the formation and breakage of contact patches between rubber-like materials and hard substrates, a semi-empirical formulation for the velocity dependence of the true interfacial shear strength τ_{s} was derived [17]:

$$\tau_{\mathrm{s}} = \tau_{\mathrm{s},0}\left(1 + \frac{E_\infty/E_0}{(1 + (\upsilon_{\mathrm{c}}/\upsilon))^n}\right), \quad (14)$$

where n is a material dependent exponent, $\tau_{\mathrm{s},0}$ is the interfacial shear strength in the limit of very low velocities, υ_{c} is the critical velocity above which the true interfacial shear strength τ_{s} reaches a plateau value, υ accounts for the sliding velocity and E_∞/E_0 is the step height of the dynamic modulus between rubbery and glassy state.

Equation (14) relates the pronounced velocity dependence of the adhesion force to interfacial peeling effects between the rubber and the substrate asperities. The rate dependence of peeling-off experiments between rubber-like materials and blunt substrates has been taken in account via the introduction of an effective surface energy $\Delta\gamma_{\mathrm{eff}}$ describing the viscoelastic nature of such processes [23, 24]. The effective surface energy $\Delta\gamma_{\mathrm{eff}}$ can be assumed to be related to the true interfacial shear strength τ_{s} via a characteristic length scale l_{s} independent of peeling rate that can be identified with the size of the peeling process zone ($l_{\mathrm{s}} \cong \Delta\gamma_{\mathrm{eff}}/\tau_{\mathrm{s}} \cong \Delta\gamma_0/\tau_{\mathrm{s},0}$). Then the rate dependence of the effective surface energy $\Delta\gamma_{\mathrm{eff}}$ follows the same semi-empirical formulation as equation (15):

$$\Delta\gamma_{\mathrm{eff}} = \Delta\gamma_0\left(1 + \frac{E_\infty/E_0}{(1 + (\upsilon_{\mathrm{c}}/\upsilon))^n}\right). \quad (15)$$

At low rates of separation, the effective surface energy exhibits a constant value corresponding to the static surface energy $\Delta\gamma_0$ which can be estimated e.g. by contact angle measurements. By increasing the rate of separation, $\Delta\gamma_{\mathrm{eff}}$ goes through a modulus-like transition and follows a power law until a critical velocity υ_{c} is reached. The step height of the transition is given by the modulus ratio observed during mechanical spectroscopy, E_∞/E_0, i.e. the ratio of the dynamic moduli in the glassy and rubbery state [24]. Similar concepts have recently been applied for the description of crack propagation in viscoelastic solids [25].

Table 1. Formulation of rubber compounds (content in phr).

Polymer	S-SBR 5025		S-SBR 2525	
content	100	100	100	100
Filler	N339	GR7000	N339	GR7000
Content	60	60	60	60
Silane	—	5	—	5
Zinc oxide	3			
Stearic acid	1			
IPPD	1.5			
CBS	2.5			
Sulfur	1.7			

3. Materials and experimental methods

A systematic variation of the formulation was carried out to separate the effect of the polymer matrix and the filler system and their impact on friction properties. Samples include a solution-styrene butadiene rubber S-SBR with 50 wt% vinyl and 25 wt% styrene (BUNA VSL 5025-0 HM) often used for tread compounds, a second solution-styrene butadiene rubber S-SBR with 25 wt% vinyl content. The polymers were mixed with two different filler systems, namely carbon black N339 and silica GR7000 with a coupling agent Coupsil 8113. The Coupsil 8113 consists of silica particles coated with a bifunctional silane, ensuring a reasonable level of dispersability during mixing and formation of covalent bonds with the polymer during vulcanization. The formulation of compounds is completed with anti-ageing (1.5 phr IPPD) as well as processing agents (1 phr stearic acid and 3 phr zinc oxide). In order to achieve a sufficient level of elasticity, both polymers were cross-linked in a steam press with 1.7 phr sulfur in combination with 2.5 phr accelerator (CBS). The full formulations of the materials are listed in table 1.

The filled elastomers had a two step mixing stage with first 5 min in an internal mixer followed by 5 min on the roller mill. The curing time was measured on a Monsanto rheometer at a temperature of 160 °C and corresponds to t95, e.g. the required time to reach 95% of the maximum torque deduced from the vulcameter curves of each compound. Test samples were finally vulcanized in a heating press under 200 bars pressure at a curing temperature of 160 °C.

The roughness analysis was carried out with a Talysurf 100 profilometer allowing a vertical range of movements of ±1 mm, which is optimal for surfaces like rough granite or fine asphalt. The horizontal interval of sampling data is $\Delta x = 0.5\ \mu$m, the vertical resolution is $\Delta z = 16$ nm. Surface measurements were carried out until the maximal length of

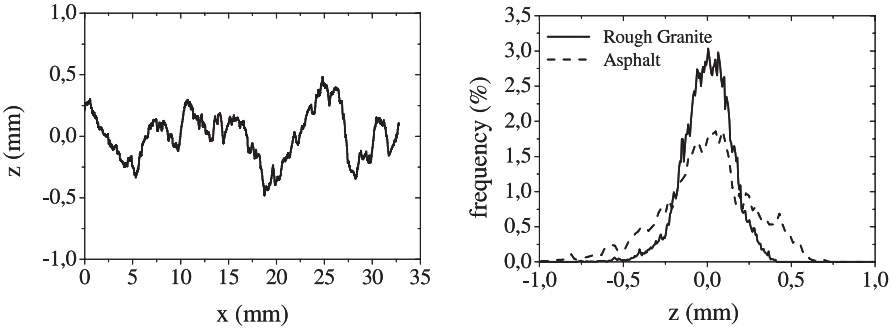

Figure 5. Profile measurement of rough granite (left) and associated normalized height distributions (right).

the traverse, e.g. 50 mm. In order to ensure a good statistic during the evaluation of surface descriptors, the measurement was repeated 10 times for each surface in different directions.

Based on a modified Zwick universal test rig, stationary friction experiments were carried out on rough surfaces under various contact conditions. Through a system of pulleys, the ensemble composed by a 2 mm thick rubber specimen glued on an aluminium plate and loaded with weights was pulled at constant velocity between $\upsilon = 0.01$ and 10 mm s^{-1} while the friction force was recorded during the test. Due to a relatively high rubber surface 50×50 mm^2, the corresponding load was found to be $\sigma_0 \sim 12$ kPa, thus preventing the occurrence of thermal and abrasion effects and a substantial modification of surface texture. Experimentally, each test was performed until the friction force reached a plateau value F_{st} characteristic of the stationary regime. The friction coefficient was then calculated as $\mu = F_{st}/F_N$, with $F_N = 30$ N.

Rough granite and asphalt were used as substrates for the friction tests. The rough granite surface was obtained after a mechanical roughening of a smooth granite specimen. A similar specimen was previously used for the study of rubber friction properties [16]. Under wet conditions, rough substrates were systematically wetted with a solution mixed with detergent in 5% concentration. The low concentration of detergent is assumed to stabilize the lubricant film at the interface and therefore prevent the occurrence of adhesion effects. Previous experimental investigations showed that a stable surfactant film is observed down to nanoscopic length scales during the contact between rubber and rigid substrate for the same range of load [26]. Moreover, the morphology of texture strongly influences the nature of contact during sliding friction. For rough substrates with sharp asperities, e.g. corundum, the addition of a small amount of detergent leads to a dramatic decrease of the wet friction coefficient over a broad range of sliding velocity, indicating that boundary lubrication occurs under wet conditions with sole water as lubricant. On the other side, the wet friction behaviour of elastomers on the currently used rough granite is not sensitive to the additon of detergent [19]. This is mainly due to a smoother morphology of texture illustrated by the ratio between horizontal and vertical cut-off length. Consequently, friction results obtained under wet conditions with detergent are identified with simulated hysteresis friction.

4. Experimental results and simulations

4.1. Roughness analysis

The characterization of rough surface is an essential step for the prediction of friction properties. A typical example is shown in figure 5 (left diagram) for a rough granite profile, whereby results are already averaged ($\langle z(x)\rangle = 0$) and levelled out ($\langle \mathrm{d}z/\mathrm{d}x\rangle = 0$). The maximal roughness amplitude peak-to-peak lies around $\Delta z_{max} = 1$ mm, which is acceptable compared to the maximum vertical stroke of the needle. The corresponding normalized height distribution $\phi(z)$ is presented in the right diagram of figure 5 together with the asphalt surface. Rough granite displays a quasi-symmetrical distribution while asphalt shows a dissymmetrical behaviour with higher roughness density over the mean value of the profile. Also the broader feature observed for the latter indicates a higher level of roughness. Both surfaces show significant advantages compared to silicon carbide based substrates which have been extensively studied during the past, namely a decrease in asperity sharpness which strongly reduces the occurrence of wear during friction process [2].

The evaluation of the height difference correlation function $C_z(\lambda)$ is presented in figure 6 for rough granite and asphalt surfaces. It physically corresponds to the average height difference of two points from a profile with increasing horizontal distance. A scaling regime can be identified at length scales comprised between the interval $\lambda = 5$–100 μm with a corresponding fractal dimension $D_2 = 2.14$. For length scales larger than $\lambda \sim 100$ μm, the path of the height difference correlation function strongly deviates from the formulated assumption which indicates the existence of a second scaling regime up to the largest length scales. By applying a fitting procedure on the upper interval $\lambda = 300$–1000 μm, a second fractal dimension $D_1 = 2.37$ can be determined. Compared to the former description with one scaling regime, the horizontal cut-off length $\xi_\parallel$ is shifted towards higher values due to the higher fractal dimension of macroroughness (from $\xi_\parallel = 1.1$ to 2.5 mm). Also, a third cut-off length λ_2 can be defined, corresponding to the intersection point of scaling ranges, namely the limit between microtexture and macrotexture. Referring to the modelling of hysteresis friction, the length scale λ_2 is associated with the boundary frequency $f = \upsilon/\lambda_2$ which delimits both friction integrals in case of a two scaling regimes approach.

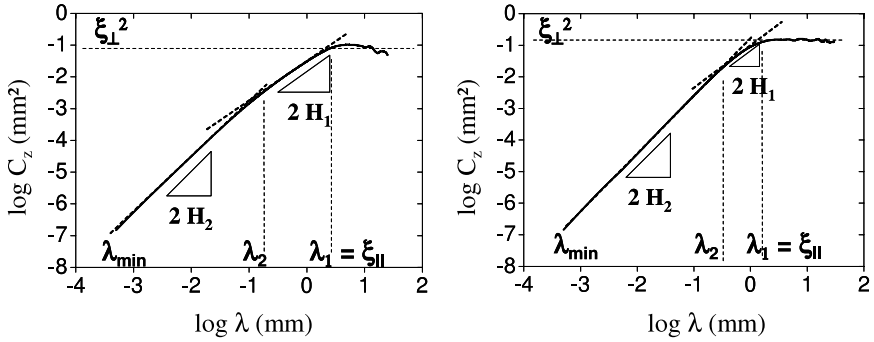

Figure 6. Average height difference correlation function $C_z(\lambda)$ for rough granite (left) and asphalt (right) with corresponding fractal descriptors.

Table 2. Surface descriptors and affine parameters for rough granite and asphalt for the one and two scaling ranges approach.

	Rough granite		Asphalt	
	1 S.R.	2 S.R.	1 S.R.	2 S.R.
D_2 (5–100 μm)	2.14	2.14	2.08	2.08
D_1 (300–1000 μm)	*x*	2.37	*x*	2.44
$\xi_\perp$ (mm)	0.31	0.31	0.38	0.38
$\xi_\parallel$ (mm)	1.06	2.49	0.90	1.55
λ_2 (mm)	*x*	0.093	*x*	0.28
s parameter	1.25	1.27	1.23	1.24

Similarly to rough granite, asphalt profile measurements were evaluated on the basis of statistical correlation functions. The corresponding height difference correlation function $C_z(\lambda)$ and surface descriptors are depicted in figure 6. Fractal analysis reveals the existence of two scaling regimes associated with distinct fractal dimensions. The microtexture is found to be related to a fractal dimension $D_2 = 2.08$ within the interval $\lambda = 5$–100 μm and a second scaling regime can be identified with $D_1 = 2.44$ within the range $\lambda = 300$–1000 μm which is associated with a cut-off length $\lambda_2 = 280$ μm. The small interval of the second scaling regime can be traced back to the nature of asphalt surfaces: indeed, the morphology of macrotexture is mainly determined by the grain size distribution, which in this case exhibits a narrow feature.

Table 2 summarizes surface descriptors with associated affine parameters obtained for rough granite and asphalt according to a one and two scaling ranges description of roughness. It should be noted that the position of the horizontal cut-off length is shifted whether the roughness is described by one or two scaling regimes—corresponding to a larger interval length for the distribution of maxima—and therefore affects the affine parameter *s*. The affine-like transformed profile was superimposed according to the mean value of the numerical height distribution, which leads to $s = 1.25$ for rough granite with a one scaling regime approach. In a similar way, the procedure was applied to asphalt and gives $s = 1.23$ (one scaling range). By describing the height difference correlation function with two scaling ranges, a slight increase of the affine parameter is observed so that one obtains $s = 1.27$ and 1.24 for the rough granite and asphalt, respectively.

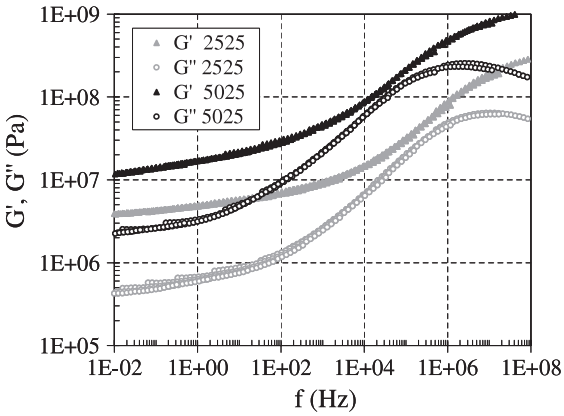

Figure 7. Master curve for carbon black filled S-SBR 5025 and S-SBR 2525 at reference temperature $T_{ref} = 23\,^\circ$C. Strain amplitude $\varepsilon = 0.5\%$.

4.2. Dynamic mechanical analysis

Results of dynamic mechanical analysis are shown in figure 7 for carbon black filled S-SBR grades at reference temperature $T_{ref} = 23\,^\circ$C and strain amplitude $\varepsilon = 0.5\%$. The storage and loss moduli, G' and G'', are depicted as a function of frequency. The dynamic glass transition is characterized by the G''-maximum located in the high frequency region. Since the high vinyl S-SBR 5025 possesses a higher glass transition temperature than the S-SBR 2525—$T_{g,5025} = -15\,^\circ$C and $T_{g,2525} = -40\,^\circ$C—the G''-maximum accordingly occurs at a lower frequency compared to the other polymer. Experimentally, frequency sweep measurements were shifted according to a generalized master procedure for filled elastomers presented in [16]. In particular, the addition of filler is related to a poor overlapping of dynamic data in the low frequency range above glass transition due to complex interactions between filler particles and surrounding polymer chains. Consequently, the classical WLF equation is completed with the introduction of vertical shift factors arising from superimposed Arrhenius-like or thermally activated processes. The corresponding activation energies were estimated for various filled composites and could be traced back to physical effects occurring on small length scales, namely the temperature dependence of immobilized polymer

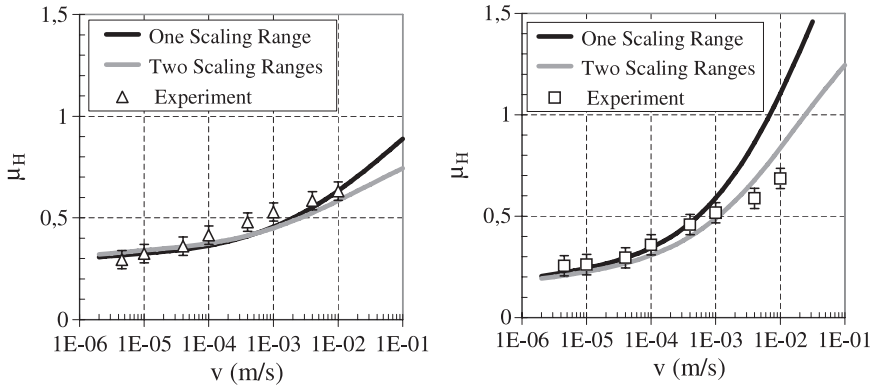

Figure 8. Wet friction results and simulated hysteresis friction for carbon black (left) and silica (right) filled S-SBR 5025 on rough granite. Load $\sigma_0 = 12.3$ kPa.

nanobridges between adjacent filler particles [16, 19, 24]. The lower activation energies of silica filled S-SBRs were interpreted as favourable behaviour for improved interlocking properties between elastomers and rough substrates. Indeed, the calculation of the real area of contact shows significant larger values for silica filled composites over a broad range of sliding velocity [16].

4.3. Implications on hysteresis friction

In the following, the impact of the multi-fractal approach on the simulated hysteresis friction is shown for filled elastomers. Furthermore, predictions are correlated with friction results obtained under wet conditions. Since the lubricant is composed of water mixed with a small amount of detergent, adhesion effects are assumed to be negligible and the experimental values are solely identified with hysteresis friction. The frequency dependent dynamic moduli required for simulations were obtained by means of mechanical spectroscopy performed at a dynamic strain amplitude $\varepsilon = 3\%$ at laboratory temperature $T = 23\,^{\circ}\mathrm{C}$ according to a novel master procedure for filled elastomers presented in [16].

Figure 8 shows friction results for carbon black and silica filled S-SBR 5025 on rough granite under wet conditions. Both compounds exhibit a continuous increase of the friction coefficient within the measuring range, with a pronounced increase of the silica filled composite. The corresponding simulations of hysteresis friction are shown on both diagrams with a differentiation made between the one and two scaling regimes approach. By considering a single scaling range, the predicted μ_H-values tend to overestimate the experimental level of wet friction with increasing sliding velocity. For example, the silica filled S-SBR 5025 shows a friction value $\mu = 0.7$ measured at a sliding velocity $\upsilon = 1$ cm s^{-1}, while the simulated hysteresis friction accounts for $\mu_H = 1.1$. A fast calculation shows that if the observed discrepancy is assumed to be solely due to the generation of heat at the interface, one would obtain a rubber temperature $T = 60\,^{\circ}\mathrm{C}$ which is unlikely to occur at moderate loads and low sliding speeds. The consideration of a second scaling regime leads to a better description of wet friction results for both filled composites. Since the extended modelling of roughness gives a finer description of the largest length scales—which actually mainly contribute to hysteresis friction—, improved correlations with wet friction behaviour can be achieved within the range of low sliding velocities.

The examination of contact parameters shows that the modelling of roughness with two scaling ranges significantly changes the picture obtained with a single scaling regime. According to equation (11), the contact interval is mainly sensitive to the exponent $\alpha = 1/(3D_2 - 6)$. By considering a second scaling range for rough granite, one obtains $\alpha \sim 0.9$ compared to $\alpha \sim 2.4$ originally. Subsequently, the smallest length scale λ_{min} contributing to hysteresis friction is shifted by about one decade with the two scaling regimes approach, thus resulting in smaller contact interval. As shown in figure 9, basic features of silica and carbon black filled S-SBR 5025 are conserved through the extended modelling since the silica filled composite exhibits lower λ_{min} values over the whole range of simulation, e.g. a favourable interlocking behaviour with the rough substrate. Finally, the predicted intersection between λ_{min} and the boundary length scale λ_2 makes clear that the impact of microtexture during sliding friction is expected to be significant under certain contact conditions, namely at low sliding velocity and high load. The reduction of the contact interval with a two scaling regimes approach has a direct consequence on the frequency range involved in the sliding process. Although the horizontal cut-off length $\xi_{\|}$ is increased through the extended modelling, the pronounced shift of λ_{min} leads to a diminution of the frequency interval by about a decade as shown in. Consequently, the flattened shape and slight shift of the μ_H maximum observed in figure 8 appear to be due to the shift and reduction of the frequency interval: while the former delays the increase of hysteresis friction, the latter confines the friction peak at a lower level.

The viscoelastic nature of hysteresis and adhesion friction is highlighted in figure 10 for carbon black filled S-SBR 5025 on rough granite. Simulations were performed at three different temperatures with a constant pre-factor $\langle\delta\rangle/\langle z_{\mathrm{p}}\rangle = 7$ according to correlations shown in figure 8. The position of the hysteresis peak is basically determined by the shift of dynamic mechanical moduli following the

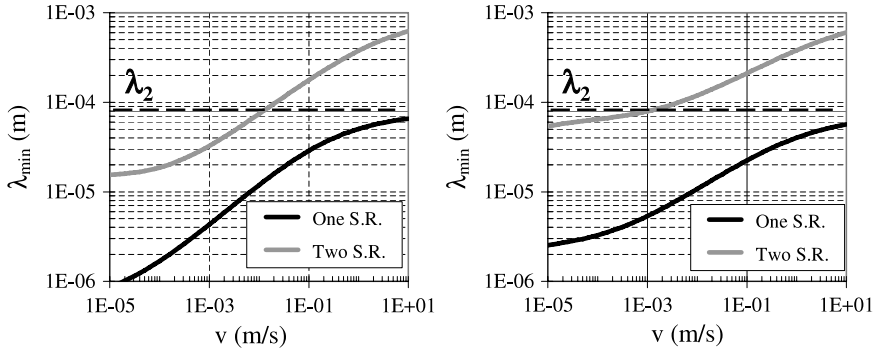

Figure 9. Simulated minimal length scale λ_{min} for silica (left) and carbon black (right) filled S-SBR 5025 on rough granite with a one and two scaling regimes approach. Load $\sigma_0 = 12.3$ kPa.

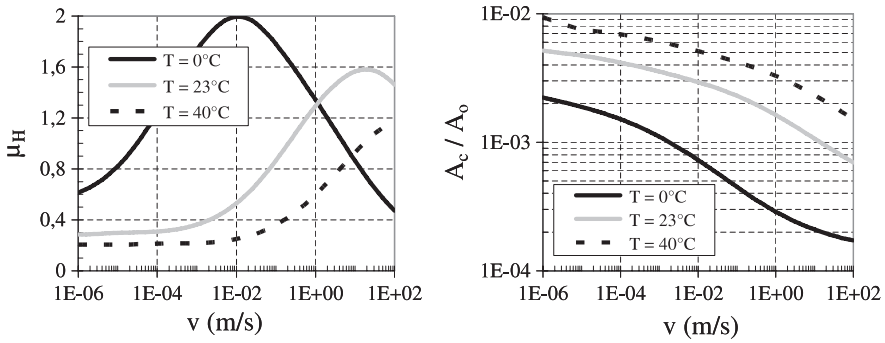

Figure 10. Simulated hysteresis friction coefficient (left) and fractional contact area (right) for carbon black filled S-SBR 5025 on rough granite at various temperatures, as indicated. Pre-factor $\langle\delta\rangle/\langle z_p\rangle = 7$. Load $\sigma_0 = 12.3$ kPa.

time–temperature superposition principle. The reduction of the hysteresis maximum with increasing temperature results from two effects. First, due to the introduction of vertical shift factors during the master procedure of filled elastomers, the level of the frequency dependent dynamic moduli drops at high reference temperatures, which subsequently reduces the amount of generated hysteresis friction. Secondly, simulations are performed under the assumption that the pre-factor is constant over the whole range of sliding velocity and temperature, which seems to be a discussible hypothesis when exploring the range of low temperature and high sliding velocity [19].

The corresponding fractional area, e.g. the ratio between the real contact area A_c and the nominal contact area A_0, is shown in the right diagram of figure 10 as a function of the sliding velocity (equation (12)). The monotonous decrease of the ratio reflects the hardening of viscoelastic materials since the spectrum of excitation frequency explores the glass transition regime with increasing sliding velocity. In addition, due to a temperature dependent softening of filled elastomers in the rubbery region, the realization of contact patches is energetically promoted with increasing temperature which finally leads to an increase of the real area of contact.

As previously shown in [16], silica filled S-SBR grades with coupling agent exhibit a higher level of adhesion friction on rough surfaces compared to carbon black filled composites. This is due to a high dynamic softening above the glass transition observed on mechanical spectroscopy results which leads to improved interlocking properties between rubber and rough surfaces. Moreover, the hysteresis friction peak is found to be more pronounced in the range of sliding velocity involved in ABS-braking phases, e.g. around $\upsilon \sim 1\ \mathrm{m\ s^{-1}}$. Consequently, improved grip properties of silica filled elastomers under dry and wet conditions can be understood and predicted on a physical basis. The examination of dry friction results in figure 11 (top) displays higher experimental values for silica filled S-SBR 2525 illustrated by the corresponding adhesion plots shown in figure 11 (bottom). The position of the adhesion maximum underlines the viscoelastic nature of peeling effects distributed within the contact area [17]. With decreasing glass transition temperature of the polymer matrix, the critical velocity υ_c of the interfacial shear strength—located near the adhesion maximum—is shifted towards high sliding velocity.

Next, simulations of hysteresis and adhesion friction gained from experimental results on rough granite are extended up to the range of high sliding velocity with a two scaling ranges approach. This is schematically shown in figure 12 for carbon black filled S-SBR 5025 on rough granite. Due to the introduction of a second scaling regime, the increase of hysteresis friction is limited up to a maximum $\mu_{H,\max} = 0.7$ reached at a sliding velocity $\upsilon_H = 0.5\ \mathrm{m\ s^{-1}}$. The adhesion friction goes through a peak associated with a critical velocity $\upsilon_c = 10^{-5}\ \mathrm{m\ s^{-1}}$ and further decreases with increasing sliding velocity. Within the range $[\upsilon_c, \upsilon_H]$, the decrease of adhesion friction combined with the increase of hysteresis friction leads

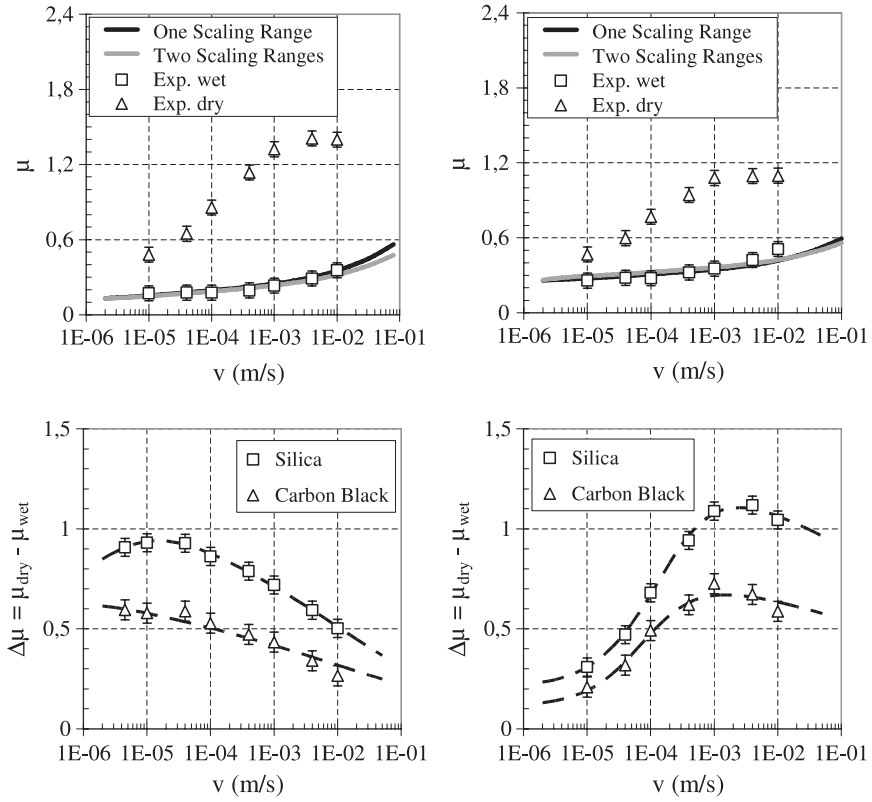

Figure 11. Top: wet and dry friction results with simulated hysteresis friction for silica (left) and carbon black (right) filled S-SBR 2525 on rough granite. Bottom: difference dry/wet for filled S-SBR 5025 (left [16]) and S-SBR 2525 (right) on rough granite with corresponding adhesion simulation (dashed lines). Load $\sigma_0 = 12.3$ kPa.

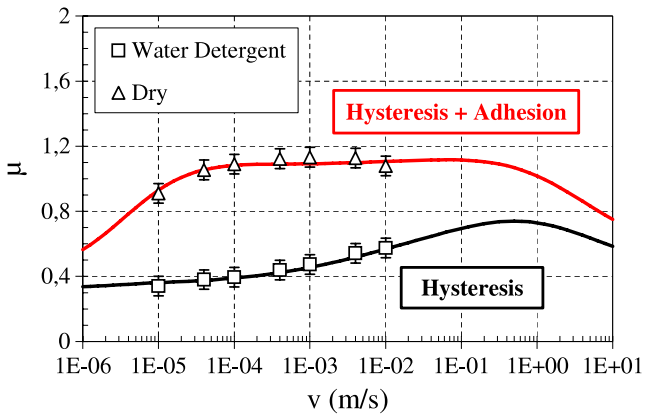

Figure 12. Extended correlations of hysteresis and adhesion friction under wet and dry conditions for carbon black filled S-SBR 5025 on rough granite.

to a constant level of dry friction illustrated by a broad maximum plateau.

By referring to previous experimental observations, the broad saturation of dry friction for filled elastomers on rough surfaces is fully predicted by a multi-scale modelling sliding friction for soft/rigid frictional pairings [2, 9]. Accordingly, the adhesion component mostly contributes to dry friction at moderate load and within the range of low sliding velocity. For the range of sliding velocity involved in tyre applications, since the occurrence of flash temperatures leads to a dramatic reduction of hysteresis friction combined with an increase of the contact area, one can reasonably expect the predominance of the adhesion contribution under dry and clean contact conditions [19].

The experimental procedure was repeated for filled S-SBR elastomers on asphalt. Figure 13 (top) shows dry and wet—water detergent—friction results, whereby wet results were compared to simulations of hysteresis friction. Similar to results previously observed on rough granite (figure 11), the modelling of roughness with a two scaling ranges approach has a slight impact on the quality of correlations for S-SBR 2525 composites since the hysteresis friction maximum is located well above the maximal measurable sliding velocity [19]. Features of adhesion friction previously observed on rough granite hold for asphalt. As shown in figure 13 (bottom), the experimental difference dry/wet is mainly determined by the polymer matrix and the filler type. Besides the influence of polymer matrix on the location of the adhesion peak, the filler system is found to control the level of adhesion via the real area of contact above critical velocity. Thereby, the dynamic mechanical softening above glass transition appears to be a key factor for the ability of rubber to fill cavity of rough profile at various length scales. Accordingly, silica filled S-SBR composites exhibit favourable interlocking properties in comparison with carbon black reinforced systems [16, 19]. The experimental procedure for the estimation of adhesion on

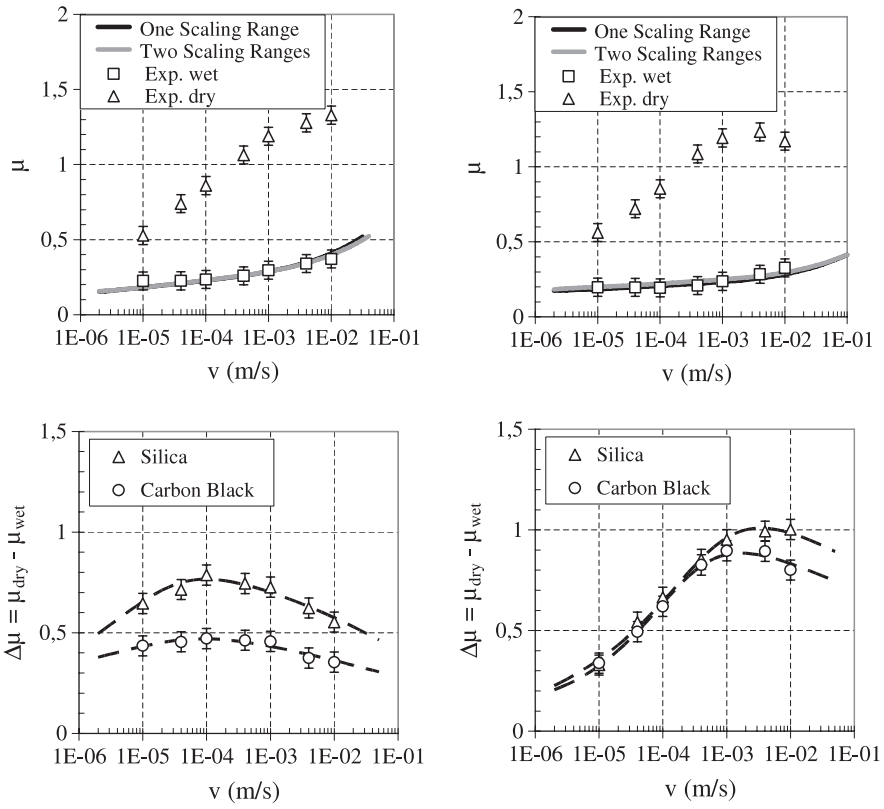

Figure 13. Top: wet and dry friction results with simulated hysteresis friction for silica (left) and carbon black (right) filled S-SBR 2525 on asphalt. Bottom: difference dry/wet for filled S-SBR 5025 (left) and S-SBR 2525 (right) on asphalt with corresponding adhesion simulation (dashed lines). Load $\sigma_0 = 12.3$ kPa.

rough surfaces confirms theoretical predictions and allows a deeper understanding of the mechanisms contributing to rubber friction on a physical basis. While the decrease of $\Delta\mu$ is clearly attributed to an effect of the real area of contact, the early increase visible below $v \sim 10^{-4}$ m s^{-1} indicates that the kinetics of peeling effects actually contributes to adhesion friction at very low sliding velocity. Similar to rough granite, the position of v_c for the silica filled S-SBR 5025 is found at a slightly higher sliding velocity than the carbon black reinforced one. Concerning the level of adhesion, no significant difference can be established between both surfaces. Compared to filled S-SBR 5025 composites, the slightly higher level of adhesion for filled S-SBR 2525 systems is attributed to the real area of contact found to be higher at a given sliding velocity.

4.4. Discussion

Numerical parameters are listed in table 3 for filled S-SBR grades on rough granite and asphalt. Since hysteresis friction is found to continuously increase within the range of low sliding velocity, the critical velocity v_c is located near the dry coefficient plateau value. A closer examination of the normalized interfacial shear strength $\tau_s/\tau_{s,max}$ extrapolated over a broad range of sliding velocity reveals a systematic variation of the position of the critical velocity with respect to the glass transition, namely a shift of the position of the adhesion peak towards high sliding velocity with decreasing

Table 3. Values of the critical velocity v_c (in m s^{-1}) and pre-factor $b = \langle\delta\rangle/\langle z_p\rangle$ for filled SBR grades on rough granite and asphalt. Load $\sigma_0 = 12.3$ kPa.

		S-SBR 5025		S-SBR 2525	
		N339	Silica	N339	Silica
v_c (m s^{-1})	Rough granite	2×10^{-6}	6×10^{-6}	4×10^{-4}	8×10^{-4}
	Asphalt	3×10^{-5}	6×10^{-5}	7×10^{-4}	10^{-3}
b	Rough granite	7	11.2	10.6	11
	Asphalt	1.1	2	1.5	2.6

glass temperature [17]. This viscoelastic feature of the adhesion component is consistent with dry friction results obtained for filled elastomers [2, 9].

Current investigations confirm the impact of glass transition temperature on the location of the critical velocity. Compared to the S-SBR 5025 polymer characterized by a glass transition temperature $T_g \sim -15\,^\circ$C, the position of v_c is shifted by around two decades for the S-SBR 2525 ($T_g \sim -40\,^\circ$C) independently of the filler type. This points out the viscoelastic nature of rubber friction on rough surfaces since a similar trend is observed on the frequency dependent dynamic moduli [17, 19]. The impact of surface roughness is indicated by a systematic shift of the values of critical velocity for asphalt. Since the velocity dependence of the interfacial shear strength is assumed to arise from the kinetics of peeling effects located at small length scales, the determining factor

for the position of υ_c seems to be the fractal dimension of microtexture.

Finally, values of the pre-factor $b = \langle\delta\rangle/\langle z_p\rangle$ are summarized in table 3. Thereby, indications of the deformed volume of elastomers during sliding friction can be gained. Silica filled composites show larger values compared to carbon black filled compounds on both surfaces which indicates that a larger amount of bulk material is involved during the indentation process by surface asperities. Based on complementary results and simulations, a discussion is proposed on a finer description of dynamic indentation processes regarding the mechanical response of filled and unfilled elastomers [19]. The impact of surface roughness on the deformed layer $\langle\delta\rangle$ is significant and the pre-factor is strongly reduced on asphalt. Numerical values of the pre-factor corroborate previous results of contact analysis carried out under static conditions [17]. Contrary to adhesion friction for which small length scales are crucial regarding the level of the real contact area and the kinetics of peeling effects, one expects the indentation behaviour to be controlled by the largest length scales of rough profile, namely the macrotexture and both cut-off lengths.

5. Conclusion

The presented modelling of hysteresis and adhesion friction allows a deeper understanding regarding the physical mechanisms involved during dynamic contact between elastomers and rough surfaces. In particular, through a separate description of the macrotexture morphology, the formulation of hysteresis friction was extended in the frame of a two scaling regimes approach. This allows the identification of the contribution of both microtexture and macrotexture on the friction coefficient under various contact conditions. As a result, the description of wet friction data is significantly improved within the range of low sliding velocity. This is due to the reduction of the contact interval in case of a two scaling regimes approach. Also, the level of adhesion friction—experimentally defined as the difference between wet and dry friction—mostly depends on the simulated real area of contact found to be significantly higher for silica filled S-SBR compared to carbon black filled composites. The position of the critical velocity shows viscoelastic features and can be tracked back to the dynamic glass transition of the elastomer. Consequently, dry friction properties of elastomers on rough surfaces are driven by three mechanisms: the length scale dependent indentation process corresponding to hysteresis friction, the dynamic filling of profile cavities by rubber—real area of contact—and the kinetics of peeling effects related to the formation and breakage of contact patches.

Acknowledgments

The authors would like to thank the Deutsche Forschung Gemeinschaft (FOR 492) for the financial support of this work. Discussions with Dr Laurent Guy (Rhodia) are appreciated.

References

[1] Payne A R 1963 *Rubber Chem. Technol.* **36** 432
[2] Grosch K A 1963 *Proc. R. Soc.* A **274** 21
[3] Heinrich G 1997 *Rubber Chem. Technol.* **70** 1
[4] Heinrich G, Klüppel M and Vilgis T A 2000 *Comput. Theor. Polym. Sci.* **10** 53
[5] Müller A, Schramm J and Klüppel M 2002 *Kautschuk Gummi Kunstst.* **55** 432
[6] Klüppel M and Heinrich G 2000 *Rubber Chem. Technol.* **73** 578
[7] Persson B N J 1998 *Sliding Friction: Physical Principles and Applications* (Berlin: Springer)
[8] Persson B N J 2001 *J. Chem. Phys.* **115** (9)
[9] Rieger H 1968 *PhD Thesis* Technische Universität Munich
[10] Kummer H W 1968 *Rubber Chem. Technol.* **41** 895
[11] Greenwood J A and Williamson J B P 1966 *Proc. R. Soc.* A **295** 300
[12] Mandelbrot B B 1982 *The Fractal Geometry of Nature* (New York: Freeman)
[13] Feder J 1988 *Fractals* (New York: Plenum)
[14] Sayles R S and Thomas T R 1978 *Nature* **271** 431
[15] Radó Z 1994 *PhD Thesis* The Pennsylvania State University
[16] Le Gal A, Yang X and Klüppel M 2005 *J. Chem. Phys.* **123** 014704
[17] Le Gal A and Klüppel M 2006 *Kautschuk Gummi Kunstst.* **65** 308
[18] Le Gal A, Guy L, Orange G, Bomal Y and Klüppel M 2007 *Wear* at press
[19] Le Gal A 2007 *PhD Thesis* University of Hannover
[20] Schramm J 2002 *PhD Thesis* University of Regensburg
[21] Westermann S, Petry F, Boes R and Thielen G 2004 *Kautschuk Gummi Kunstst.* **57** 645
[22] Heinrich G and Klüppel M 2007 *Wear* submitted
[23] Barquins M 1992 *Wear* **158** 87
[24] de Gennes P G 1996 *Langmuir* **12** 4497
[25] Persson B N J and Brener E A 2005 *Phys. Rev.* E **71** 036123
[26] Richards S C and Roberts A D 1992 *J. Phys. D: Appl. Phys.* **25** A76–80